


 Cite this: *Lab Chip*, 2023, 23, 3002

Bioengineering of a human physiologically relevant microfluidic blood–cerebrospinal fluid barrier model†

 Ying Zhou,^{‡a} Haowen Qiao,^{‡b} Fang Xu,^{‡b} Wen Zhao,^b Jibo Wang,^b Longjun Gu,^b Pu Chen ^{*b} and Mian Peng ^{*ac}

The human blood–cerebrospinal fluid barrier (hBCSFB) plays a crucial role in regulating brain interstitial fluid homeostasis, and disruption of the hBCSFB is associated with various neurological diseases. Generation of a BCSFB model with human physiologically relevant structural and functional features is crucial to reveal the cellular and molecular basis of these diseases and discover novel neurologic therapeutic agents. Unfortunately, thus far, few humanized BCSFB models are available for basic and preclinical research. Here, we demonstrate a bioengineered hBCSFB model on a microfluidic device constructed by co-culturing primary human choroid plexus epithelial cells (hCPECs) and human brain microvascular endothelial cells (hBMECs) on the two sides of a porous membrane. The model reconstitutes tight junctions of the hBCSFB and displays a physiologically relevant molecular permeability. Using this model, we further generate a neuropathological model of the hBCSFB under neuroinflammation. Overall, we expect that this work will offer a high-fidelity hBCSFB model for studying neuroinflammation-related diseases.

 Received 16th February 2023,
 Accepted 24th May 2023

DOI: 10.1039/d3lc00131h

rsc.li/loc

Introduction

Human brain function relies on the homeostasis of the central nervous system (CNS), which is maintained by continuous substance exchange and segregation of neurotoxic proteins, immune cells and pathogens in the peripheral circulation. The blood–brain barrier (BBB) and blood–cerebrospinal fluid barrier (BCSFB) are two major loci that execute the transfer and barrier function of the brain.¹ Distinct from the BBB composed of microvascular endothelial cells, pericyte cells, and astrocytic end-feet in the brain parenchyma, the BCSFB consists of a convoluted layer of choroid plexus (ChP) epithelium and fenestrated capillary loops, floating in the ventricles.^{1,2} More than a tight barrier separating cerebrospinal fluid (CSF) from blood, the BCSFB actively produces CSF and transports various molecules through its unique transport and secretory system.¹ In

addition, the BCSFB provides a unique neuro-immunological interface due to its expression of adhesion molecules and chemokines that facilitate immune cell migration.^{3–5}

Because of these unique properties, human blood–cerebrospinal fluid barrier (hBCSFB) dysfunction has been regarded as one of the major causes of various neurological diseases. Coronavirus disease 2019 (COVID-19), a fatal acute respiratory syndrome caused by SARS-CoV-2, has been reported to manifest neurological complications.^{6,7} Although its pathophysiological mechanism remains unclear, the disruption of the hBCSFB plays a pivotal role in the neurological infection of SARS-CoV-2 during acute COVID-19.^{8,9} In addition, the deposition of β -amyloid has been proven to be associated with the impaired clearance ability of ChP epithelium in Alzheimer's disease.^{10–12}

Although recent progress in non-invasive imaging techniques has facilitated functional assessment of the hBCSFB, they are mainly applied to evaluate CSF dynamics.^{13–15} Mechanistic understanding of the role of the hBCSFB in neuropathological processes relies on animal and cell culture models. Mice models are frequently used for studying the BCSFB; however, their gene expression and functional annotation are different from humans.¹⁶ For example, aquaporin-4 (AQP4), a predominant water-selective transporter that contributes to brain water dynamics, is expressed on the human ChP epithelium but mainly detected in the ependymal and subependymal regions of mice.¹⁷ Current developments of three-dimensional (3D) *in vitro*

^a Department of Anesthesiology, Zhongnan Hospital of Wuhan University, Wuhan 430071, China. E-mail: mianpeng@whu.edu.cn

^b Tissue Engineering and Organ Manufacturing (TEOM) Lab, Department of Biomedical Engineering, Wuhan University TaiKang Medical School (School of Basic Medical Sciences), Wuhan 430071, China. E-mail: puchen@whu.edu.cn

^c Brain Research Center, Zhongnan Hospital of Wuhan University, Wuhan 430071, China

 † Electronic supplementary information (ESI) available. See DOI: <https://doi.org/10.1039/d3lc00131h>

‡ These authors contributed equally to the article.

models, such as inverted Transwell systems and stem cell-derived ChP organoids, advance studies of functional and systemic responses of the BCSFB.^{18–20} However, existing cultured cell models still fail to reconstitute the *in vivo*-like fluidic microenvironment, which will limit their utility and translation to the patients.

In recent years, organ-on-chip technology has provided a high-fidelity *in vitro* model system to recapitulate the structural and functional features of human tissue barriers.²¹ It allows the reconstitution of the biomechanical and biochemical micro-environment of tissue barriers in the aspects of cellular polarization, cell–cell interfaces, local hemodynamics, and molecular permeability.²² To date, a variety of human tissue barriers have been emulated, including the BBB,²³ blood–retina barrier,^{24,25} pulmonary endothelial barrier,^{26–28} and blood–testis barrier.^{29,30} These models not only demonstrate similar structures to those *in vivo* but also possess tissue-barrier specific functions.

Here, we design a microfluidic system for establishing a hBCSFB model *in vitro*. Two microchannels are segregated by transparent polyester (PET) porous membranes, which are sandwiched between human-derived ChP epithelial cells and brain microvascular endothelial cells. The two microchannels were continually perfused with microfluid. This device reproduces the cytoarchitecture and barrier function of the hBCSFB and fills the gap in the existing BCSFB models. Using this model, we demonstrate that neuropathology forms in the hBCSFB when it is exposed to inflammatory stimuli, which is present in a variety of neurological conditions.

Materials and methods

Microfluidic chip fabrication

The design of the microdevice used for the hBCSFB-on-chip model was modified from a previously reported BBB-on-chip.³¹ The chip was composed of two parallel and closely opposed microchannels that were cast in polydimethylsiloxane (PDMS) elastomer. Briefly, the PDMS mixture at a 10:1 mass ratio of base agent to curing agent was poured onto the photolithographically prepared SU-8 microchannel masters and was fully degassed at –80 kPa. Subsequently, the prepolymer of PDMS was cured at 65 °C for 4 h. The fully cured PDMS construct was peeled off from the masters and cut into separate parts embossed with microchannels. The upper and lower channels were 2 cm long and 1 mm wide; 200 and 100 μm high, respectively. Therefore, the total area in the microfluidic device for cell growth was 0.2 cm². Four holes punched by a biopsy punch with a 1 mm diameter in the upper parts of the microdevices were used as inlets and outlets of the hBCSFB-on-chip. PET membranes (0.4 μm perpendicular pores at a density of 2 × 10⁶ pores per cm²) were bonded to the surface of the lower parts to separate the channels. Then, the upper and lower parts were aligned and bonded to each other under a stereomicroscope by hand.

Cell culture

The primary human choroid plexus epithelial cells (hCPECs) and primary human brain microvascular endothelial cells (hBMECs) were both purchased from Sciencell (cat #1310, #1000), and propagated in a T25 flask for passage and cryopreserved according to the manufacturer's instructions. To minimize experimental variability, only the primary cells in passages 3–6 were used for experiments.

HBCSFB reconstitution on the microfluidic chips

Before cell seeding, the channels of the microfluidic chips were coated with Matrigel (800 μg ml^{–1}, Corning) for the “ventricle channel” and laminin (100 μg ml^{–1}, Sigma) for the “blood channel” overnight at 37 °C. Both channels were rinsed with DPBS and then with their specific media before seeding cells. For culturing hBMECs in the “blood channel”, hBMECs at a seeding density ranging between 0.5 and 1 × 10⁷ cells per ml were introduced into the lower compartment of the microchannel, and the microdevice was flipped immediately to allow the hBMECs to attach to the laminin-coated membrane. After incubating at 37 °C, 5% CO₂ for 4 h, the microfluidic chip was flipped back. Then, hCPECs were introduced into the upper compartment at a concentration ranging between 1 and 3 × 10⁷ cells per ml, and incubated overnight at 37 °C and 5% CO₂. On the next day of cell seeding, the microfluidic chips were connected to the peristaltic pump, and both channels were continuously perfused with fresh media at 30 μl h^{–1}. To test for the responses of hBCSFB-on-chip to inflammatory stimulation, tumor necrosis factor α (TNF-α) (PeproTech, AF-300-01A) was perfused through the lower channel on day 4 for 24 h.

Numerical simulation

The numerical model based on the finite element method was established to predict the flow field in the two channels of the hBCSFB-on-chip. The permeability of the interface was adjusted between the channels to simulate the absence or presence of hBMECs. According to the porous zone assumption,³² the void fraction of the porous membrane (ε) was calculated from the following equation:

$$\varepsilon = \frac{\pi \rho d^2}{4} \quad (1)$$

Here d is the hole diameter and ρ is the pore density. Since the CSF is considered to be an incompressible, viscous Newtonian fluid, Darcy's law is satisfied in the hBCSFB-on-chip, ignoring diffusion and convective acceleration:

$$\nabla P = -\frac{\mu}{\alpha} \vec{v} \quad (2)$$

where P is the pressure, μ is the viscosity, α is the permeability, and v is the velocity. To calculate the porosity of the PET membrane, the permeability was adjusted to 2.5 × 10^{–16} m^{–2} or 2.5 × 10^{–17} m^{–2} in the absence or presence of cells attached to the membrane.³³ The CSF velocity and

pressure fields throughout the hBCSFB-on-chip were calculated by solving the Navier–Stokes and Darcy flow equations:

$$\rho(\mathbf{v} \cdot \nabla)\mathbf{v} = \nabla \cdot [-p\mathbf{I} + \mathbf{k}] \quad (3)$$

where k is the permeability, and I is the hydraulic gradient. All these simulations were conducted on COMSOL Multiphysics (COMSOL Inc., Burlington, MA, USA). The “free and porous media flow” module was utilized to model the fluid motion in the microchannel. Specifically, the “porous media” condition was used to define the properties of the porous membrane, and the void fraction of the porous membrane was set according to eqn (1). Moreover, the “mass transport” module was used to simulate the nutrient diffusion from the lower channel to the upper channel, and the “diffusion coefficient” in the fluid was set to $5.15 \times 10^{-10} \text{ m}^2 \text{ s}^{-1}$. The CSF velocity and pressure fields throughout the hBCSFB-on-chip were calculated after creating meshes and defining boundaries. A steady-state solver was used to determine the velocity, fluidic shear stress, streamlines, and pressure in the microchannels.

Immunofluorescence staining

HBMECs and hCPECs in the microchannels were fixed with 4% paraformaldehyde for 15 min at room temperature and then washed with DPBS. Next, cells were blocked in 10% goat serum in DPBS with 0.5% Triton X-100 for 1 h. The primary antibodies used in the study were transthyretin (TTR) (1:100, Abclonal, A1120), CD31 (1:100, Abcam, ab24590), AQP1 (1:100, Abcam, ab219055), zona occludens-1 (ZO-1) (1:200, Proteintech, 21773-1-AP), and glucose transporter-1 (Glut-1) (1:100, Proteintech, A6982). After incubation with the primary antibodies overnight at 4 °C, cells were incubated with Alexa Fluor-488, Alexa Fluor-647, or Cy-3 secondary antibodies (1:300, all from Invitrogen) for 1 h at room temperature. The nuclei of both types of cells were then counterstained with DAPI (Life Technologies). Images were captured with a Leica TCS SP8 STED confocal microscope equipped with LAS X software. Quantitative analysis of immunofluorescence images was conducted using the ImageJ software (NIH, MD, USA). Briefly, each fluorescence image was obtained with background subtraction and then converted into a binary image. The expression of target proteins was presented as the average mean fluorescent intensity (MFI), which was computed using eqn (4):

$$\text{MFI} = \frac{\text{integrated optical density (IOD) of target protein}}{\text{total area}} \quad (4)$$

Permeability assessment

To evaluate the barrier function, the apparent permeability (P_{app}) of hBCSFB-on-chip was calculated by a previously

described method.³⁴ All the P_{app} assays were performed by perfusing the upper and lower channels with a medium flow of $30 \mu\text{l h}^{-1}$. NaFl-FITC (0.376 kDa, Sigma, F6377) and dextran-Texas Red (10 kDa, Invitrogen, D1828) were dissolved in the hBMEC medium at a concentration of $10 \mu\text{g ml}^{-1}$ and $100 \mu\text{g ml}^{-1}$, respectively, and either of these tracers was perfused through the lower channel for 12 h. Meanwhile, the upper channel was perfused with the hCPEC medium. The medium was collected from inlets and outlets of both the upper and lower channels. The concentrations of NaFl and dextran in the effluents from both channels were evaluated by a multifunctional plate reader (INFINITE 200 PRO). To calculate P_{app} , the following equation (eqn (5)) was used:

$$P_{\text{app}} = \frac{(\text{Top Output } (\mu\text{g ml}^{-1}) - \text{Top Input } (\mu\text{g ml}^{-1}))}{(\text{Bottom Input } (\mu\text{g ml}^{-1}))} \quad (5)$$

$$\times \frac{(\text{Flow Rate } (\text{ml s}^{-1}))}{\text{Membrane area } (\text{cm}^2)}$$

To test the permeability of protein, human IgG (Abcam, ab205806) was used in place of NaFl/dextran. Quantitation of IgG in the “ventricle channel” was performed using the IgG Human ELISA kit (ELK Biotechnology, ELK 1390).

Transcriptional analysis

The hCPECs in each condition (2D monoculture, hBCSFB-on-chip culture or hBCSFB-on-chip treated with TNF- α) were collected on day 5 ($n = 4-5$). Specifically, hCPECs in three hBCSFB-on-chips were pooled as one sample to meet the cell numbers needed for RNA sequencing. For sample preparation, hCPECs were washed gently with $1 \times$ DPBS, and then the total RNA was extracted using TRIzol (Abclonal, RK30129) according to the manufacturer's instructions. The collected samples were submitted to Novogene Bioinformatics Technology Co, Beijing, China, for library preparation and transcriptome sequencing. After quality control and RNA-seq library preparation, the samples were sequenced using Illumina Next Seq6000, with an average of 20 million reads per run. The differentially expressed genes (DEGs) were selected by the following thresholds: adjusted (adj) p -value < 0.05 and $|\log_2\text{FoldChange}| > 1$. The GO (Gene Ontology) and KEGG (Kyoto Encyclopedia of Genes and Genomes) pathway enrichment analysis were performed using DAVID (<https://david.ncifcrf.gov/>).

Results

Construction of hBCSFB-on-chip

The HBCSFB consists of monolayered ChP epithelium and fenestrated capillaries (Fig. 1A). Thus, a microfluidic chip with two layered microchannels was employed in the present study to reconstitute the cellular components of the hBCSFB and its extracellular environment *in vitro* (Fig. 1B). We used soft lithography to create flexible, transparent microfluidic devices containing two parallel microchannels that can be perfused simultaneously. The microchannels were partitioned

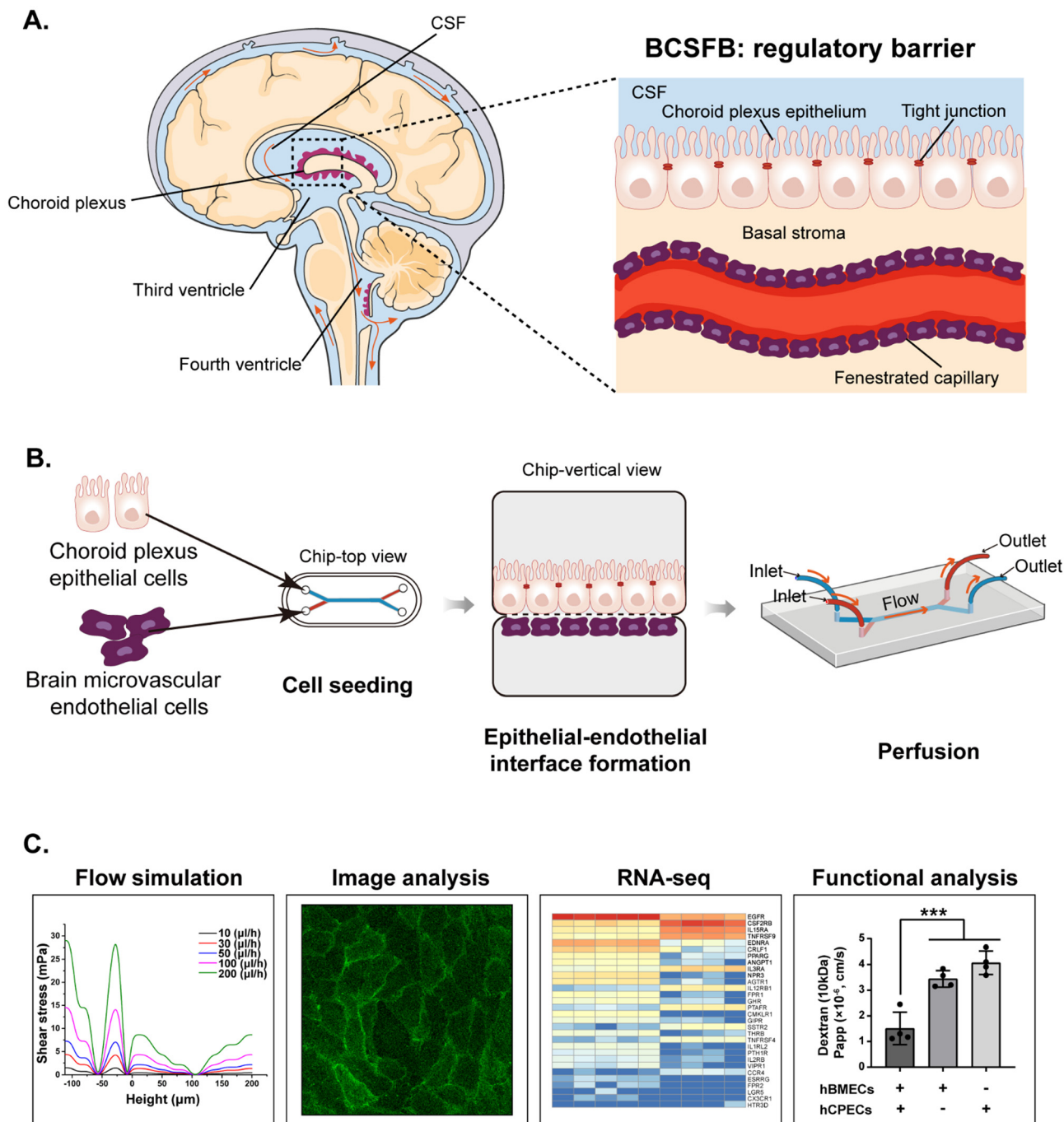


Fig. 1 Schematic diagram of the generation of the hBCSFB-on-chip model. (A) Schematic representation of the BCSFB in the human brain. (B) The schematic overview of the experimental procedures of hBCSFB-on-chip. BMECs were initially seeded in the lower channel of the hBCSFB-on-chip, while the hCPECs were seeded in the upper channel. Following cell attachment, both channels were perfused continuously with fresh medium. (C) The phenotype and function of the BCSFB were analyzed using the different indicated methods.

by a porous PET membrane, which served as the cellular interface between hCPECs and hBMECs (Fig. 1B). Following cell attachment, fresh medium was continuously introduced to both of the microchannels to mimic the dynamic flow of CSF and blood (Fig. 1B). Therefore, the proposed hBCSFB-on-chip system provided a simple and efficient platform to reconstruct a humanized BCSFB model in the present study (Fig. 1C).

Biomechanical analysis of fluid dynamics in the hBCSFB-on-chips

To better understand and quantify the fluid flow in the hBCSFB-on-chip, a numerical simulation was conducted upon a model constructed with the realistic chip geometries (Fig. 2A and B). A range of velocity was used to simulate the physiologically fluidic environment in the hBCSFB-on-chip. The

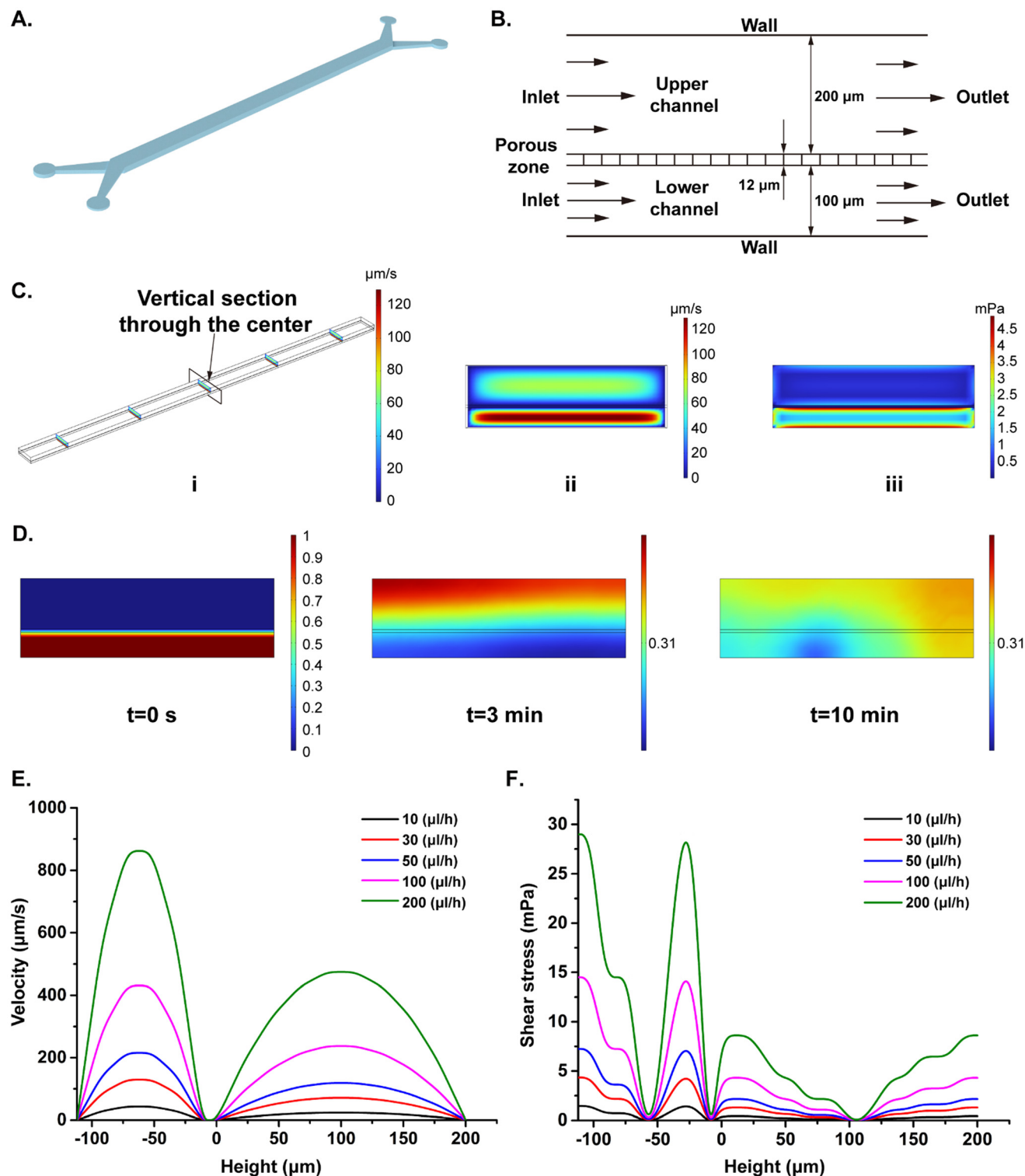


Fig. 2 Numerical modeling and simulations of the hBCSFB-on-chip. (A) Geometric modeling of the hBCSFB-on-chip. (B) Geometric size of the hBCSFB-on-chip. (C) Simulation results of the velocity (ii) and shear stress (iii) at the vertical section through the center of the hBCSFB-on-chip (i). (D) Simulation results of molecule diffusion from the lower channel to the upper channel in the vertical direction over time. (E) Distribution analysis results of the velocity. (F) Distribution analysis results of the shear stress.

vertical section through the center of the hBCSFB-on-chip was selected as a representative sample for analysis (Fig. 2C-i). In all flow velocity conditions, the velocity distribution in the two

channels was symmetrical (Fig. 2C-ii), and the shear stress was mainly concentrated at the membrane on which the cells were planted (Fig. 2C-iii). Furthermore, the mass transport and

efficient diffusion of molecules from the lower channel (“blood channel”) to the upper channel (“ventricle channel”) over time were proved by COMSOL simulation (Fig. 2D), which indicates that the medium exchange can be achieved in our hBCSFB-on-chip model. The quantitative analysis was conducted to determine the velocity and fluidic shear stress. The velocities at different initial flow rates all presented a parabolic distribution in either the upper or lower channel and fitted with the porous media flow (Fig. 2E), which is consistent with those *in vivo*. Then we calculated the shear stress under different initial flow rates, and found that the maximum shear stress was distributed on the channel wall of the hBCSFB-on-chip and porous membrane rather than the center of the channel (Fig. 2F). In addition, the shear stress value, 0.32–4.35 mPa (Fig. 2C-iii), generated under a flow rate of 30 $\mu\text{l h}^{-1}$ is within the physiological range.³⁵ In the absence of cell attachment in the membrane, the fluid can penetrate through the porous membrane down to the lower channel near the inlet region (Fig. S1A†). It proved the connectivity between the two channels in the simulation model and presented a parabolic profile at a stable state (Fig. S1B†). In addition, the velocity distribution on the section also conforms to the characteristics of laminar flow (Fig. S1C and D†). These results provide a clue for the flow field inside the channels, which is critical for understanding mass transfer under fluid flow and biomechanical effects during the culture medium exchange.

Co-cultured hCPECs and hBMECs under laminar flow express tissue-specific markers of the hBCSFB

In the living organism, the BCSFB is exposed to two circulating fluids, the blood and CSF. Therefore, both the hCPECs and hBMECs were stimulated by laminar flow at a rate of 30 $\mu\text{l h}^{-1}$ (Fig. 3A). Plated hCPECs in the upper channel formed a monolayer that expressed its specific marker TTR, while hBMECs in the lower channel, on the opposite of the PET membrane, expressed the endothelial marker CD31 (Fig. 3B). After 5 days of microfluidic culture, cells in both of the channels were still attached to the porous PET membrane, forming an epithelial–endothelial interface (Fig. 3C). To assess whether the dynamic extracellular environment can functionalize the *in vitro* model of the hBCSFB in this study, we examined the expression of tight junction proteins, as well as major transporters of hCPECs. As shown in Fig. 3D, the tight junction marker ZO-1 formed the cell-to-cell junction along cell borders. The glucose transporter Glut-1 and the water transporter AQP1, which are important transporters to maintain the metabolic homeostasis of the brain,¹ were detected on hCPECs as well (Fig. 3D). We also tested the surface topography of the hBCSFB, and observed that hCPECs formed microvilli-like subcellular structures on the apical membrane in the hBCSFB-on-chip, which are similar to the ChP *in vivo* (Fig. 3E). Together, these results demonstrated that the laminar flow enhanced the formation of the functional structures in the hBCSFB-on-chip.

HBCSFB-on-chip recapitulates the physiologically-relevant transcriptomic signature and form a selective barrier

To test whether laminar flow and interaction with hBMECs can promote the functionality of hCPECs, we used the global RNA-sequencing (RNA-seq) analysis to compare the transcriptome differences between hCPECs cultured in the hBCSFB-on-chip and hCPECs under conventional 2D monoculture. The DEG analysis identified a total of 5298 genes that were significantly differentially expressed, with 2737 up-regulated and 2561 down-regulated transcripts in hCPECs under 3D microfluidic culture compared to the control (Fig. 4A). Then, we performed gene ontology (GO) enrichment analysis to highlight the different cellular locations, molecular functions, and biological processes. The GO enrichment analysis of the DEG data was classified into four major functional categories: angiogenesis-related pathways (Fig. 4B), cell–cell junction-related pathways (Fig. 4C), membrane assembly-related pathways (Fig. 4D), and transport function-related pathways (Fig. 4E). The sub-categories of GO assignments with the largest transcripts were ‘angiogenesis’, ‘cell–substrate junction’, and ‘membrane region’. The upregulation of the barrier and transport function of hCPECs in hBCSFB-on-chip was also confirmed by the increased mRNA expression of Claudin-5 (CLD5) and Glut-1 in hCPECs cultured in the hBCSFB-on-chip as compared to the controls (Fig. 4F). Furthermore, the upregulated expression levels of several representative transporters of the hBCSFB (Fig. S2A–L†), such as ATP binding cassette transporter G1 (ABCG1, cholesterol transporter), ABCB1 (P-Glycoprotein) and solute carrier family 19 member 1 (SLC19A1, folate transporter), were also detected in the hCPECs cultured in the hBCSFB-on-chip. Considering that the hBCSFB acts as a highly active transport interface with high local blood flow,³⁶ these results prompt us to imply that our model closely recapitulates the functional features of the BCSFB in the human brain.

To further verify the functionality of the hBCSFB-on-chip, we assessed whether molecules with different molecular weights could be selectively filtered. Notably, compared to hCPECs or hBMECs cultured alone in the microdevices under dynamic conditions, the permeability of the hBCSFB-on-chip was significantly decreased for dextran (10 kDa) but not NaFl (0.376 kDa) (Fig. 4G and H), indicating that the size-dependent transport capacity was recapitulated in the hBCSFB-on-chip system. Taken together, these results demonstrate that hBCSFB-on-chip recreates some physiologically-relevant functions, which are also in line with previous studies showing that dynamic flow can improve the biological properties of cells.^{34,37}

TNF- α induces the dysfunction in the hBCSFB-on-chip

The breakdown of the BCSFB induced by systemic inflammation has been documented in various neurological disorders.^{38–40} Therefore, we perfused the “blood channel” with TNF- α , a classic inflammatory cytokine, to test the validation of hBCSFB-on-chip in disease modeling (Fig. 5A). We determined the dysfunction in the hBCSFB-on-chip after

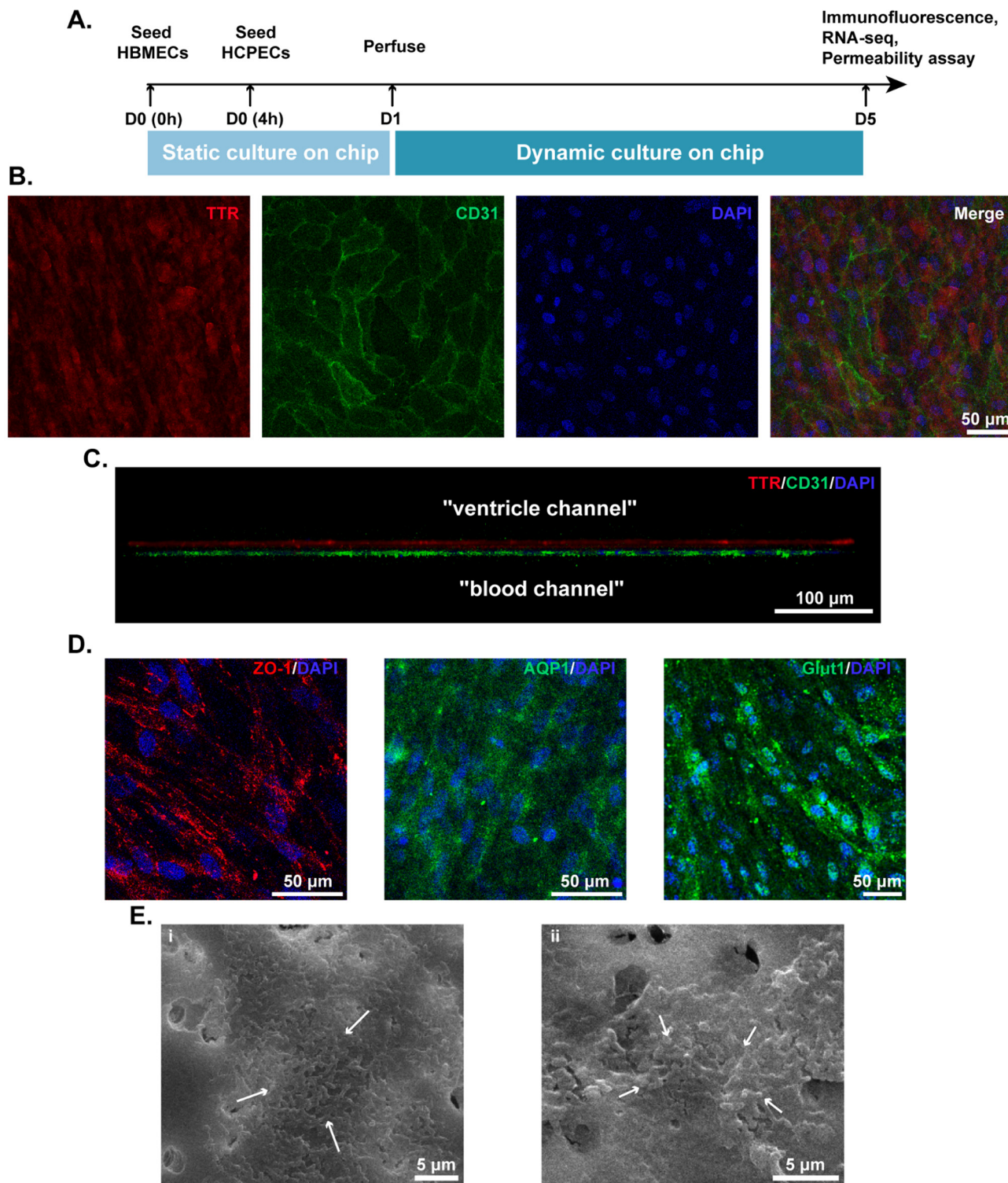


Fig. 3 Characterization of hBCSFB-on-chip. (A) Timeline of the experimental protocol. (B) Immunofluorescence images of the hBCSFB-on-chip on day 5 under perfused condition. hCPECs are immunostained for their specific cellular marker TTR (red), and hBMECs are immunostained for CD31 (green). Scale bar, 50 μm . (C) The hCPECs (TTR, red; DAPI, blue) and hBMECs (CD31, green) grow on the opposite sides of the PET membrane in the hBCSFB-on-chip, forming an epithelial–endothelial interface. Scale bar, 100 μm . (D) hCPECs grown in the “ventricle channel” of the hBCSFB-on-chip express the choroid plexus epithelial cell markers ZO-1, AQP1, and Glut1. Scale bar, 50 μm . (E) Electron micrographs of microvilli on the hCPECs (indicated by arrows) on day 5 under perfused condition. Scale bars represent 5 μm in i and ii.

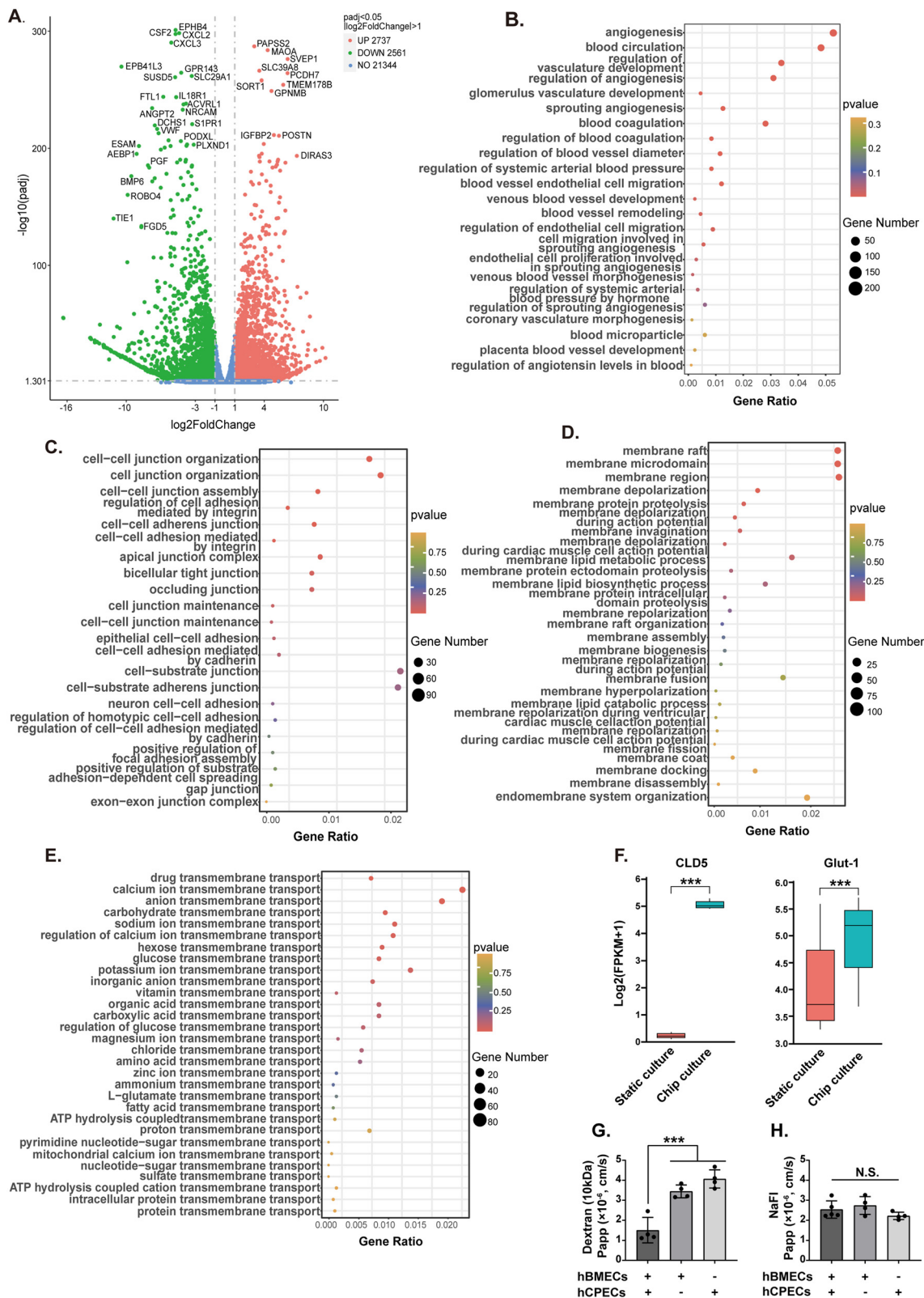


Fig. 4 HBCSFB-on-chip recapitulates the physiologically relevant transcriptomic signature and forms a selective barrier. (A) The volcano plot depicts differential gene expression in hCPECs which are co-cultured with hBMECs under laminar flow compared to the controls which are cultured alone under static conditions. (B–E) Bubble plots of GO gene set enrichment analysis of all the differentially expressed genes in hCPECs cultured in the hBCSFB-on-chip. Y-Axis labels represent the enrichment components, and the gene ratio score is shown on the X-axis. The size of the bubble represents the number of genes assigned in each pathway, and the color accords with the enrichment significance. (F) Box plots of RNA-seq analysis showing expression levels of CLD5 and Glut-1. Permeability of dextran (10 kDa) (G) and NaFl (0.376 kDa) (H) were compared in hBCSFB-on-chips seeded with hBMECs and hCPECs, hBMECs alone, or hCPECs alone. *** $p < 0.001$.

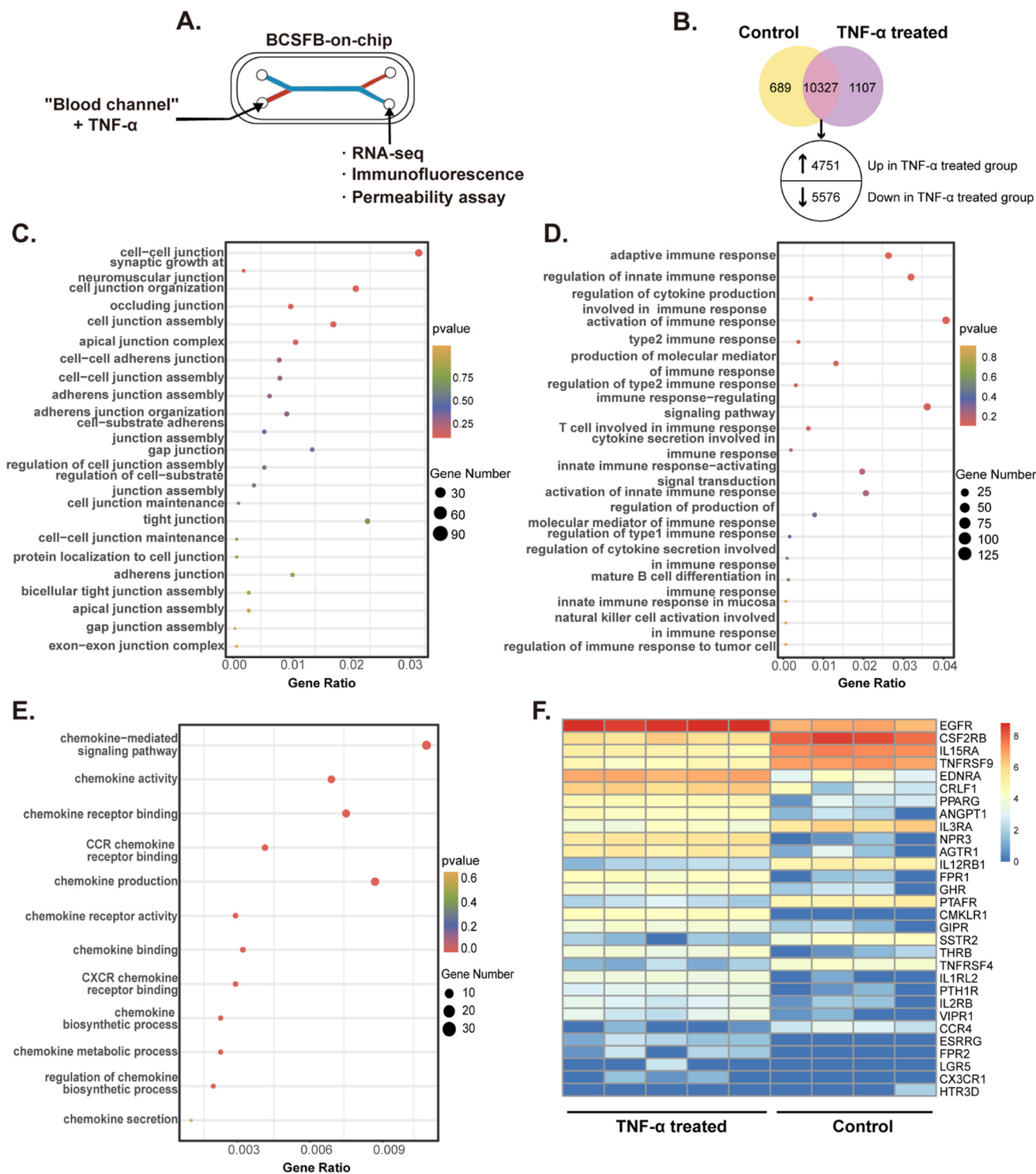


Fig. 5 Transcriptional profiling of hCPECs in the hBCSFB-on-chip upon inflammatory stimulation. (A) Schematic graph of perfusion of TNF- α through the hBCSFB-on-chip. (B) Venn diagram of genes in hCPECs treated with TNF- α or in control condition. (C–E) Bubble plots of GO gene set enrichment analysis for upregulated and downregulated genes in hCPECs derived from the TNF- α treated hBCSFB-on-chips compared to the controls. (F) Heatmap of log₂ expression values of differentially expressed gene datasets of hCPECs in TNF- α treated hBCSFB-on-chips compared to the controls.

the exposure to TNF- α . Gene list comparison identified that TNF- α treatment resulted in 1107 unique, 4751 up-regulated and 5576 down-regulated DEGs in hCPECs compared to the

untreated control, as shown in a Venn diagram (Fig. 5B). GO enrichment analysis revealed the association of the DEGs in the cell-cell junction (Fig. 5C), angiogenesis (Fig. S3A[†]),

membrane assembly (Fig. S3B[†]), and transport function (Fig. S3C[†]) when compared to the controls. The most striking finding was that the TNF- α treatment specifically regulated genes with a key role in innate immune responses. These genes principally belong to the categories of immune response families (Fig. 5D), chemokine-mediated pathways (Fig. 5E), and cytokine process-related pathways (Fig. S3D[†]). Moreover, the comparative analysis showed the top 30 genes related to inflammatory responses (Fig. 5F).

We next assessed whether transcriptomic changes were associated with the disruption of the tight junction protein ZO-1. Immunofluorescence staining analysis demonstrated barrier damage following exposure to inflammatory factors TNF- α (Fig. 6A–C). Next, we conducted permeability assays on the hBCSFB-on-chip upon exposure to inflammatory factors. Our data indicate significantly increased permeability to immunoglobulins (IgG) and dextran in the brain channel of the hBCSFB-on-chip on 5 days after exposure to inflammatory factors (Fig. 6D and E). All these data suggest that the hBCSFB-on-chip could be used to assess biochemical treatments for inflammatory stimuli.

Discussion

In the present study, we combined reverse bioengineering and organ-on-chip technologies to develop a hBCSFB-on-chip system that could closely resemble the ChP fluid environment. Specifically, we constructed a microfluidic device to produce a bionic BCSFB-like structure by incorporating BCSFB-specific dynamic culture, and multicellular architectures, composed of hCPECs and hBMECs. Additionally, the hBCSFB-on-chip demonstrated a physiological response to inflammatory cues at the tissue level.

Microfluidic technologies have offered unprecedented opportunities to bioengineer various tissues by recapitulating their key features of structures and functionalities. In our current study, we took two fundamental properties of the human BCSFB into account: a functional cytoarchitecture and barrier function, and employed optimized hBCSFB-on-chip combined with bioengineering to reproduce such properties of human ChP. This hBCSFB-on-chip system could recreate some crucial features *in vivo* like ChP multicellular

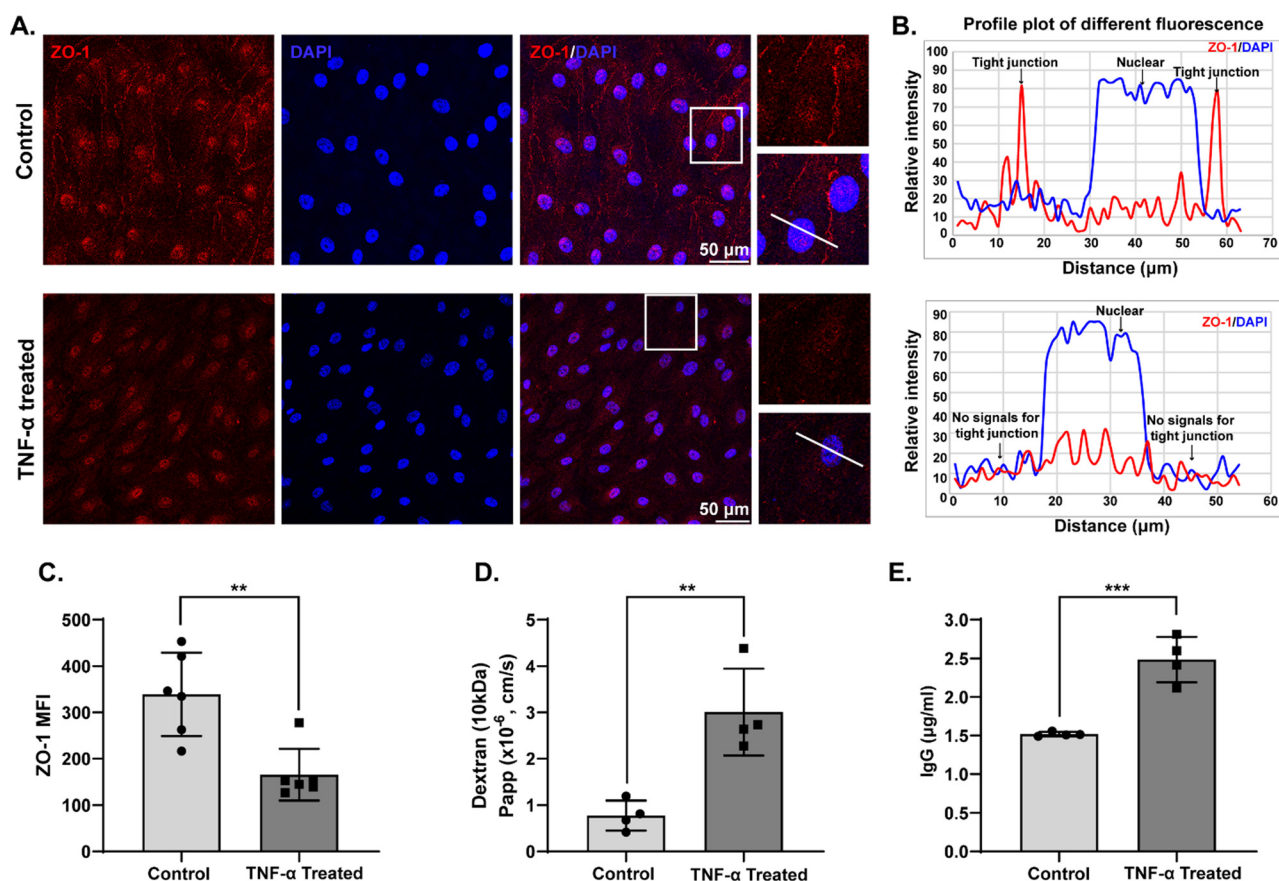


Fig. 6 TNF- α treatment disrupts the barrier function of the hBCSFB-on-chip. (A) Immunofluorescence staining of hCPECs in hBCSFB-on-chip for ZO-1 and DAPI. Boxed regions showed that the expression of ZO-1 on hCPECs was reduced by TNF- α treatment. Scale bar, 50 μ m. (B) The profile of ZO-1 (red) and DAPI (blue) represented the distribution and relative intensity of fluorescence based on the distance shown on the lines in (A). (C) Image-based quantification of the ZO-1 expression in the hCPECs cultured in TNF- α treated hBCSFB-on-chips and the controls. (D and E) Permeability of dextran (10 kDa) and IgG following perfusion of TNF- α showed impaired barrier function of hBCSFB-on-chips. ** p < 0.01, *** p < 0.001.

architectures and tissue-barrier interfaces by incorporating parallel microchannels. Specifically, the hBMEC seeding in the bottom channel formed a tight monolayer to constitute the “blood channel”, and primary hCPECs were seeded on the top to form the “ventricle channel”. A flexible, porous membrane, coated with the tissue-relevant extracellular matrix, separates the endothelial cells from the hCPECs cultured independently in a specific medium with controlled laminar flow and shear stress. Assessing the interaction of integrated hBCSFB-on-chip showed that hBMECs marked by CD31 formed a uniform monolayer on the “blood channel”, while hCPECs expressing TTR formed an intricate network within the brain compartment. The BCSFB is an important secretory structure in the brain, and to that end, it has numerous solute and water transporters, as well as efflux transporters. The expression of Glut1 glucose transporter, water transporter AQP-1, and tight junctional complex ZO-1 in hCPECs cultured in the hBCSFB-on-chip reflected the specialization of ChP function. SEM analysis showed that hCPECs contain villus-like microstructures, which mirrors the ChP structure in the real human situation. Furthermore, compared with monocultured hCPECs or hBMECs, the integrated hBCSFB-on-chip by co-culturing with hCPECs and hBMECs significantly decreased the blood-to-brain leakage of dextran. Gene expression profiling of integrated hBCSFB-on-chip and single-cultured hCPECs showed robust differences. Additionally, GO enrichment analysis of the DEGs showed highly enriched categories related to angiogenesis, cell–cell junction, membrane assembly, and transport-related functions in the integrated hBCSFB-on-chip. Importantly, we detected upregulation of nutrient trafficking-specific transporters in the hCPECs in the hBCSFB-on-chip model, including ABCG1 and SLC19A1. Considering that ChP plays a unique role in the transport of cholesterol and folate,^{41,42} our model may provide a tool for studying the role of the BCSFB in maintaining CNS homeostasis. In addition, ABCB1, namely multidrug resistance protein 1, is an active efflux pump for numerous drugs, including chemotherapeutic agents, antipsychotics, and HIV protease inhibitors.^{43–45} Thus, our model may also serve as an effective tool for screening drug candidates that are able to transport through the human BCSFB. Notably, ChP organoids have recently emerged as an invaluable research model system for recapitulating the morphology and function of human ChP.^{9,20} The ChP organoids are derived from human embryonic stem cells (hESCs) or human induced pluripotent stem cells (hiPSCs), and they often start from homogeneous primitive neuroectoderm to intricate ChP barrier architecture with a fluid-filled compartment. Because organoid generation is based on the accumulating knowledge of developmental biology, these models are very suitable for exploring different developmental stages of ChP. Additionally, the ChP organoids do not contain any vasculature, which is a disadvantage for the studies aimed at oxygen transport and nutrient delivery. Therefore, our hBCSFB-on-chip model and ChP organoids represent distinct approaches based on the strategies of

bioengineering and developmental biology, respectively. These two different CNS barrier models can supplement each other with their benefits. Taken together, the bioengineered hBCSFB-on-chip provided human physiologically relevant *in vitro* and clinically relevant models, recapitulating the structural and functional features of the BCSFB barrier.

Although both the BBB and BCSFB are major players in mediating CNS homeostasis, the importance of the BCSFB is underestimated compared to the BBB. Structurally, the BBB is sealed by tight junction complexes among adjacent endothelial cells, resulting in a low permeability to most of the molecules in the peripheral blood. In contrast, the endothelial membrane on the BCSFB interface has leaky inter-endothelial junctions and forms fenestrations. Thus, the BCSFB is more permeable than the BBB.² In the present study, the permeability of hBCSFB-on-chip was higher than that of the previously reported BBB-on-chip,³⁴ which is consistent with the physiological condition. More importantly, the unique expression of adhesion molecules, chemokines, and cytokines on the BCSFB make it act as a positive immunosurveillance system in the brain.⁴⁶ The ChP participates in neuro-humoral brain modulation and neuroimmune interactions, thereby contributing greatly to maintaining brain homeostasis. Based on this hBCSFB-on-chip model, we further investigated the neuropathology of the BCSFB under inflammatory stimuli. TNF- α is a pleiotropic pro-inflammatory cytokine and a key mediator involved in several pathological conditions. What is more, TNF- α is reported as the main inflammatory upstream mediator in ChP tissue in AD patients. In our study, the hBCSFB-on-chip could be used to model TNF- α induced functional damage at the BCSFB tight junctions. TNF- α was perfused at a physiologically relevant shear stress through the “blood channel”, while the ventricle compartment with hCPECs was perfused with normal media. Interestingly, we observed the loss of tight junctions in the hCPECs, as shown by the decreased expression of ZO-1, suggesting the breakdown of the BCSFB barrier. These results suggested that the BCSFB interface established in our model mimicked functional responses to inflammatory stimulations applied on the “blood channel”. In addition, the RNA-seq was also performed to guide the investigation of the regulatory effects of TNF- α stimulation on the signaling pathways related to the barrier function, including the angiogenesis, cell–cell junction, membrane assembly, and transport-related functions. The ChP-CSF system is key to brain homeostasis, waste clearance, and immune regulations. However, it remains elusive how TNF- α affects the immune system in the BCSFB. Here, we used hBCSFB-on-chip to study the different effects of TNF- α induced inflammatory responses. We observed a significant difference in intracellular signaling mediated after the TNF- α treatment. GO enrichment analysis classified the functional categories of DEGs, in terms of immune response families, chemokine-mediated pathways, and cytokine process-related pathways. This indicated that the complex BCSFB environment in our system resulted in

robust stimulation of immune response, which was consistent with the notion that ChP served as a crucial source for brain homeostasis and immune regulations in the brain. Thus, this new BCSFB model more closely recapitulates the human immune response in ChP and allows us to address the significance of TNF- α induced inflammatory pathways. Overall, our novel hBCSFB-on-chip provides a unique opportunity to investigate human BCSFB function under inflammatory stimuli, and a potential platform for drug screening.

Despite the above advantages, this hBCSFB-on-chip has some limitations. As we mentioned earlier, the BCSFB orchestrates the neuroimmune interactions through its ability to facilitate immune cell migration.³⁶ For example, recent studies have documented the migration of specific T lymphocyte subsets through the BCSFB in multiple sclerosis.^{47,48} However, the co-culture with immune cells in our BCSFB-on-chip model has not been achieved in the present study, which might be due to the impact of cell culture medium. A more complicated co-culture system that includes immune cells or brain parenchymal cells should be developed further. As the identification and validation of disease-specific pathology remain a considerable challenge, we anticipate that a variety of experimental approaches will be possible to overcome these limitations. Overall, we believe that our hBCSFB-on-chip system utilized in the current work could serve as an alternative human-relevant model, and open a new avenue for modeling BCSFB disorders.

Author contributions

Conceptualization: M. P., P. C. Data curation: M. P., P. C. Formal analysis: H. Q., Y. Z., F. X. Funding acquisition: M. P., P. C. Investigation: Y. Z., H. Q., F. X. Methodology: Y. Z., F. X., W. Z., H. Q., L. G. Project administration: M. P., P. C. Resources: M. P., P. C. Simulation: F. X., J. W., H. Q. Supervision: M. P., P. C. Validation: J. W., W. Z. Visualization: Y. Z., H. Q., F. X. Writing – original draft: Y. Z., H. Q., F. X. Writing – review & editing: M. P., P. C.

Conflicts of interest

There are no conflicts to declare.

Acknowledgements

This work was supported by grants from the National Natural Science Foundation of China (81870851, 82071208), the Outstanding Talented Young Doctor Program of Hubei Province (HB20200407), the Translational Medicine, and interdisciplinary Research Joint Fund of Zhongnan Hospital of Wuhan University (ZNJC202012), the Medical Sci-Tech Innovation Platform of Zhongnan Hospital of Wuhan University (PTXM2022019), and the Medical Science Advancement Program (Clinical Medicine) of Wuhan University (TFLC 2018003).

References

- Z. Redzic, *Fluids Barriers CNS*, 2011, **8**, 3.
- C. E. Johanson, E. G. Stopa and P. N. McMillan, in *The Blood-Brain and Other Neural Barriers: Reviews and Protocols*, ed. S. Nag, Humana Press, Totowa, NJ, 2011, pp. 101–131, DOI: [10.1007/978-1-60761-938-3_4](https://doi.org/10.1007/978-1-60761-938-3_4).
- I. Strominger, Y. Elyahu, O. Berner, J. Reckhow, K. Mittal, A. Nemirovsky and A. Monsonego, *Front. Immunol.*, 2018, **9**, 1066–1066.
- J. H. Mills, L. M. Alabanza, D. A. Mahamed and M. S. Bynoe, *J. Neuroinflammation*, 2012, **9**, 193–193.
- G. Kunis, K. Baruch, N. Rosenzweig, A. Kertser, O. Miller, T. Berkutzki and M. Schwartz, *Brain*, 2013, **136**, 3427–3440.
- A. Varatharaj, N. Thomas, M. A. Ellul, N. W. S. Davies, T. A. Pollak, E. L. Tenorio, M. Sultan, A. Easton, G. Breen, M. Zandi, J. P. Coles, H. Manji, R. Al-Shahi Salman, D. K. Menon, T. R. Nicholson, L. A. Benjamin, A. Carson, C. Smith, M. R. Turner, T. Solomon, R. Kneen, S. L. Pett, I. Galea, R. H. Thomas, B. D. Michael, C. Allen, N. Archibald, J. Arkell, P. Arthur-Farraj, M. Baker, H. Ball, V. Bradley-Barker, Z. Brown, S. Bruno, L. Carey, C. Carswell, A. Chakrabarti, J. Choulerton, M. Daher, R. Davies, R. Di Marco Barros, S. Dima, R. Dunley, D. Dutta, R. Ellis, A. Everitt, J. Fady, P. Fearon, L. Fisniku, I. Gbinigie, A. Gemski, E. Gillies, E. Gkrania-Klotsas, J. Grigg, H. Hamdalla, J. Hubbett, N. Hunter, A.-C. Huys, I. Ihmoda, S. Ispoglou, A. Jha, R. Joussi, D. Kalladka, H. Khalifeh, S. Kooij, G. Kumar, S. Kyaw, L. Li, E. Littleton, M. Macleod, M. J. Macleod, B. Madigan, V. Mahadasa, M. Manoharan, R. Marigold, I. Marks, P. Matthews, M. McCormick, C. McInnes, A. Metastasio, P. Milburn-McNulty, C. Mitchell, D. Mitchell, C. Morgans, H. Morris, J. Morrow, A. Mubarak Mohamed, P. Mulvenna, L. Murphy, R. Namushi, E. Newman, W. Phillips, A. Pinto, D. A. Price, H. Proschel, T. Quinn, D. Ramsey, C. Roffe, A. Ross Russell, N. Samarasekera, S. Sawcer, W. Sayed, L. Sekaran, J. Serra-Mestres, V. Snowdon, G. Strike, J. Sun, C. Tang, M. Vrana, R. Wade, C. Wharton, L. Wiblin, I. Boubriak, K. Herman and G. Plant, *Lancet Psychiatry*, 2020, **7**, 875–882.
- T. Moriguchi, N. Harii, J. Goto, D. Harada, H. Sugawara, J. Takamino, M. Ueno, H. Sakata, K. Kondo, N. Myose, A. Nakao, M. Takeda, H. Haro, O. Inoue, K. Suzuki-Inoue, K. Kubokawa, S. Ogihara, T. Sasaki, H. Kinouchi, H. Kojin, M. Ito, H. Onishi, T. Shimizu, Y. Sasaki, N. Enomoto, H. Ishihara, S. Furuya, T. Yamamoto and S. Shimada, *Int. J. Infect. Dis.*, 2020, **94**, 55–58.
- F. Jacob, S. R. Pather, W.-K. Huang, F. Zhang, S. Z. H. Wong, H. Zhou, B. Cubitt, W. Fan, C. Z. Chen, M. Xu, M. Pradhan, D. Y. Zhang, W. Zheng, A. G. Bang, H. Song, J. Carlos de la Torre and G.-L. Ming, *Cell Stem Cell*, 2020, **27**, 937–950.e939.
- L. Pellegrini, A. Albecka, D. L. Mallery, M. J. Kellner, D. Paul, A. P. Carter, L. C. James and M. A. Lancaster, *Cell Stem Cell*, 2020, **27**, 951–961.e955.
- M. Brkic, S. Balusu, E. Van Wonterghem, N. Gorlé, I. Benilova, A. Kremer, I. Van Hove, L. Moons, B. De Strooper,

- S. Kanazir, C. Libert and R. E. Vandenbroucke, *J. Neurosci.*, 2015, **35**, 12766–12778.
- 11 F. Bartolome, A. Krzyzanowska, M. de la Cueva, C. Pascual, D. Antequera, C. Spuch, A. Villarejo-Galende, A. Rabano, J. Fortea, D. Alcolea, A. Lleo, I. Ferrer, J. Hardy, A. Abramov and E. Carro, *Sci. Rep.*, 2020, **10**, 9391.
- 12 C. Spuch, D. Antequera, C. Pascual, S. Abilleira, M. A. Blanco, M. A. J. Moreno-Carretero, J. S. Romero-López, T. Ishida, J. A. Molina, A. Villarejo, F. Bermejo-Pareja and E. Carro, *Front. Cell. Neurosci.*, 2015, **9**, 134.
- 13 P. G. Evans, M. Sokolska, A. Alves, I. F. Harrison, Y. Ohene, P. Nahavandi, O. Ismail, E. Miranda, M. F. Lythgoe, D. L. Thomas and J. A. Wells, *Nat. Commun.*, 2020, **11**, 2081.
- 14 C. Perera, D. Tolomeo, R. R. Baker, Y. Ohene, A. Korsak, M. F. Lythgoe, D. L. Thomas and J. A. Wells, *Front. Mol. Neurosci.*, 2022, **15**, 964632.
- 15 L. R. Sass, M. Khani, J. Romm, M. Schmid Daners, K. McCain, T. Freeman, G. T. Carter, D. L. Weeks, B. Petersen, J. Aldred, D. Wingett and B. A. Martin, *Fluids Barriers CNS*, 2020, **17**, 4.
- 16 S. F. Janssen, S. J. van der Spek, J. B. Ten Brink, A. H. Essing, T. G. Gorgels, P. J. van der Spek, N. M. Jansonius and A. A. Bergen, *PLoS One*, 2013, **8**, e83345.
- 17 F. Deffner, C. Gleiser, U. Mattheus, A. Wagner, P. H. Neckel, P. Fallier-Becker, B. Hirt and A. F. Mack, *Cell. Mol. Life Sci.*, 2022, **79**, 90.
- 18 A. D. Monnot and W. Zheng, *Methods in molecular biology*, Clifton, N.J., 2013, vol. 945, pp. 13–29.
- 19 T. Tenenbaum, T. Papandreou, D. Gellrich, U. Friedrichs, A. Seibt, R. D. Adam, C. Wewer, H.-J. Galla, C. Schwerek and H. Schrotten, *Cell. Microbiol.*, 2009, **11**, 323–336.
- 20 L. Pellegrini, C. Bonfio, J. Chadwick, F. Begum, M. Skehel and M. A. Lancaster, *Science*, 2020, **369**, eaaz5626.
- 21 Y. Zhao, U. Demirci, Y. Chen and P. Chen, *Lab Chip*, 2020, **20**, 1531–1543.
- 22 S. N. Bhatia and D. E. Ingber, *Nat. Biotechnol.*, 2014, **32**, 760–772.
- 23 A. Oddo, B. Peng, Z. Tong, Y. Wei, W. Y. Tong, H. Thissen and N. H. Voelcker, *Trends Biotechnol.*, 2019, **37**, 1295–1314.
- 24 Y. B. Arık, W. Buijsman, J. Loessberg-Zahl, C. Cuartas-Vélez, C. Veenstra, S. Logtenberg, A. M. Grobbink, P. Bergveld, G. Gagliardi, A. I. den Hollander, N. Bosschaart, A. van den Berg, R. Passier and A. D. van der Meer, *Lab Chip*, 2021, **21**, 272–283.
- 25 J. Yeste, M. García-Ramírez, X. Illa, A. Guimerà, C. Hernández, R. Simó and R. Villa, *Lab Chip*, 2018, **18**, 95–105.
- 26 P. Zamprogno, S. Wüthrich, S. Achenbach, G. Thoma, J. D. Stucki, N. Hobi, N. Schneider-Daum, C.-M. Lehr, H. Huwer, T. Geiser, R. A. Schmid and O. T. Guenat, *Commun. Biol.*, 2021, **4**, 168.
- 27 V. V. Thacker, K. Sharma, N. Dhar, G.-F. Mancini, J. Sordet-Dessimoz and J. D. McKinney, *EMBO Rep.*, 2021, **22**, e52744.
- 28 N. Roldan, A. Rapet, G. Raggi, M. Epars, K. Fytianos, J. D. Stucki, N. Schneider-Daum, C. Michael-Lehr, H. Huwer, T. Geiser, O. T. Guenat and N. Hobi, *Eur. Respir. J.*, 2019, **54**, OA1903.
- 29 S. Sharma, B. Venzac, T. Burgers, S. Schlatt and S. Le Gac, *Organs-on-a-Chip*, 2022, **4**, 100023.
- 30 A. AbuMadighem, S. Shuchat, E. Lunenfeld, G. Yossifon and M. Huleihel, *Biofabrication*, 2022, **14**, 035004.
- 31 T.-E. Park, N. Mustafaoglu, A. Herland, R. Hasselkus, R. Mannix, E. A. FitzGerald, R. Prantil-Baun, A. Watters, O. Henry, M. Benz, H. Sanchez, H. J. McCrea, L. C. Goumnerova, H. W. Song, S. P. Palecek, E. Shusta and D. E. Ingber, *Nat. Commun.*, 2019, **10**, 2621.
- 32 J. J. Stickel and A. Fotopoulos, *Biotechnol. Prog.*, 2001, **17**, 744–751.
- 33 Y. Du, N. Li, H. Yang, C. Luo, Y. Gong, C. Tong, Y. Gao, S. Lü and M. Long, *Lab Chip*, 2017, **17**, 782–794.
- 34 G. D. Vatine, R. Barrile, M. J. Workman, S. Sances, B. K. Barriga, M. Rahnama, S. Barthakur, M. Kasendra, C. Lucchesi, J. Kerns, N. Wen, W. R. Spivia, Z. Chen, J. Van Eyk and C. N. Svendsen, *Cell Stem Cell*, 2019, **24**, 995–1005. e1006.
- 35 S. Yamada, H. Ito, M. Ishikawa, K. Yamamoto, M. Yamaguchi, M. Oshima and K. Nozaki, *AJNR Am. J. Neuroradiol.*, 2021, **42**, 479–486.
- 36 J.-F. Gherzi-Egea, N. Strazielle, M. Catala, V. Silva-Vargas, F. Doetsch and B. Engelhardt, *Acta Neuropathol.*, 2018, **135**, 337–361.
- 37 S.-S. D. Carter, L. Barbe, M. Tenje and G. Mestres, *Biomater. Sci.*, 2020, **8**, 6309–6321.
- 38 B. R. Ott, R. N. Jones, L. A. Daiello, S. M. de la Monte, E. G. Stopa, C. E. Johanson, C. Denby and P. Grammas, *Front. Aging Neurosci.*, 2018, **10**, 245.
- 39 K. Baruch, N. Ron-Harel, H. Gal, A. Deczkowska, E. Shifrut, W. Ndifon, N. Mirlas-Neisberg, M. Cardon, I. Vaknin, L. Cahalon, T. Berkutzki, M. P. Mattson, F. Gomez-Pinilla, N. Friedman and M. Schwartz, *Proc. Natl. Acad. Sci. U. S. A.*, 2013, **110**, 2264–2269.
- 40 E. G. Stopa, K. Q. Tanis, M. C. Miller, E. V. Nikonova, A. A. Podtelezchnikov, E. M. Finney, D. J. Stone, L. M. Camargo, L. Parker, A. Verma, A. Baird, J. E. Donahue, T. Torabi, B. P. Eliceiri, G. D. Silverberg and C. E. Johanson, *Fluids Barriers CNS*, 2018, **15**, 18.
- 41 M. Fujiyoshi, S. Ohtsuki, S. Hori, M. Tachikawa and T. Terasaki, *J. Neurochem.*, 2007, **100**, 968–978.
- 42 J. B. Wollack, B. Makori, S. Ahlawat, R. Koneru, S. C. Picinich, A. Smith, I. D. Goldman, A. Qiu, P. D. Cole, J. Glod and B. Kamen, *J. Neurochem.*, 2008, **104**, 1494–1503.
- 43 V. V. Rao, J. L. Dahlheimer, M. E. Bardgett, A. Z. Snyder, R. A. Finch, A. C. Sartorelli and D. Piwnica-Worms, *Proc. Natl. Acad. Sci. U. S. A.*, 1999, **96**, 3900–3905.
- 44 J. Wijnholds, E. C. M. de Lange, G. L. Scheffer, D.-J. van den Berg, C. A. A. M. Mol, M. van der Valk, A. H. Schinkel, R. J. Scheper, D. D. Breimer and P. Borst, *J. Clin. Invest.*, 2000, **105**, 279–285.
- 45 O. Osborne, N. Peyravian, M. Nair, S. Daunert and M. Toborek, *Trends Neurosci.*, 2020, **43**, 695–708.
- 46 M. Ayub, H. K. Jin and J. S. Bae, *BMB Rep.*, 2021, **54**, 196–202.

- 47 H. Nishihara, S. Soldati, A. Mossu, M. Rosito, H. Rudolph, W. A. Muller, D. Latorre, F. Sallusto, M. Sospedra, R. Martin, H. Ishikawa, T. Tenenbaum, H. Schrotten, F. Gosselet and B. Engelhardt, *Fluids Barriers CNS*, 2020, **17**, 3.
- 48 S. Rodríguez-Lorenzo, J. Konings, S. van der Pol, A. Kamermans, S. Amor, J. van Horsen, M. E. Witte, G. Kooij and H. E. de Vries, *Acta Neuropathol. Commun.*, 2020, **8**, 9.